



Deposited via The University of York.

White Rose Research Online URL for this paper:

<https://eprints.whiterose.ac.uk/id/eprint/233989/>

Version: Published Version

Article:

Gao, Yang, Ji, Ruipeng, Ren, Ziyi et al. (2025) Insights into the Synergistic Mechanism of a Polyol-Assisted Ternary Deep Eutectic Solvent for the Production of Lignocellulosic Nanofibers and Lignin Nanoparticles from Sunflower Stalks. *ACS Sustainable Chemistry & Engineering*. pp. 19586-19598. ISSN: 2168-0485

<https://doi.org/10.1021/acssuschemeng.5c07767>

Reuse

This article is distributed under the terms of the Creative Commons Attribution (CC BY) licence. This licence allows you to distribute, remix, tweak, and build upon the work, even commercially, as long as you credit the authors for the original work. More information and the full terms of the licence here:

<https://creativecommons.org/licenses/>

Takedown

If you consider content in White Rose Research Online to be in breach of UK law, please notify us by emailing eprints@whiterose.ac.uk including the URL of the record and the reason for the withdrawal request.

Insights into the Synergistic Mechanism of a Polyol-Assisted Ternary Deep Eutectic Solvent for the Production of Lignocellulosic Nanofibers and Lignin Nanoparticles from Sunflower Stalks

Yang Gao,* Ruipeng Ji, Ziyi Ren, Zhicheng Jiang, Shichao Xu,* and Avtar S. Matharu*



Cite This: <https://doi.org/10.1021/acssuschemeng.5c07767>



Read Online

ACCESS |

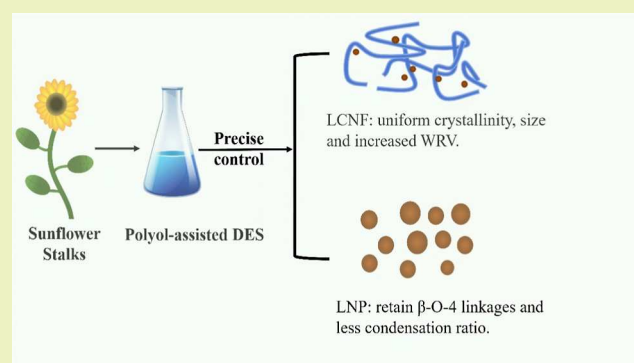
Metrics & More

Article Recommendations

Supporting Information

ABSTRACT: The use of traditional acidic deep eutectic solvents (DESs) causes substantial lignin condensation and thus limits the subsequent downstream valorization of lignocellulosic biomass into lignocellulosic nanofibers (LCNFs) and lignin nanoparticles (LNPs). Herein, a ternary DES comprising choline chloride, lactic acid, and one of three polyols (glycerol, 1,2-propanediol, or ethylene glycol) is evaluated for its efficacy to produce LCNFs and LNPs from sunflower stalks, a high-volume renewable resource. The incorporation of polyols decreased the solvent acidity and led to a reduction in delignification. The resultant LCNFs had uniform crystallinity (36.34–41.49%), uniform size dispersity (13.46–18.84 nm diameter), and their water retention value (WRV) increased from 16.3 to 21.7% on increasing the polyol content. Simultaneously, LNPs recovered from polyol-assisted DES pretreatment retained aromatic ring structures and exhibited a spherical morphology with particle sizes between 23.52 and 63.26 nm. Interestingly, the LNPs displayed moderate and homogeneous molecular weights and preserved β -O-4 substructures, while the degree of condensation decreased significantly from 21.8 to 10.3%, highlighting the stabilization effect of polyols. In conclusion, this study demonstrates the significant potential of polyol-assisted ternary DESs for the sustainable and high-quality production of lignocellulosic nanomaterials from sunflower stalks.

KEYWORDS: DES, polyols, LCNF, LNP, sunflower stalks



1. INTRODUCTION

It is now well documented that our historic and continued reliance on petrochemical resources for chemicals, materials, and energy has adversely impacted climate change and global sustainability.^{1,2} Thus, there are now global concerted efforts toward the development of sustainable, carbon-neutral, and zero waste biorefineries reliant on underutilized renewable resources to address future chemical, material, and energy demands. Underutilized or spent lignocellulosic biomass, primarily composed of cellulose, hemicellulose, and lignin, has garnered significant interest as an alternative to crude oil due to its abundance rich chemical functionality and interesting physicochemical properties.^{3–5} However, the intricate cross-linked chemical architecture of lignocellulose renders the cellulose as a recalcitrant thus severely limiting its extraction and downstream valorisation.⁶ Thus, the effective pretreatment of lignocellulosic biomass has been recognized as a critical step in the development of economically viable, zero-waste, and second-generation integrated biorefineries.⁷

The use of deep eutectic solvents (DESs) is recognized as a promising pretreatment strategy for lignocellulosic biomass owing to their low cost, facile preparation, nonvolatile nature, biodegradability, and recyclability.^{8–10} DES are eutectic

mixtures of a hydrogen-bond donor (HBD) and a hydrogen-bond acceptor (HBA) at defined molar ratios, resulting in melting points lower than those of the individual components.¹¹ DES cleaves the β -O-4 ether linkages in lignin-carbohydrate complexes and thus is capable of selectively extracting lignin from lignocellulosic feedstocks. However, DES pretreatment continues to encounter key challenges such as their inherently high viscosity impedes mass transfer and limits intraparticle penetration during extraction.¹²

There are many studies reported in the literature that use DES for biomass fractionation, either solely or in combination with a third component, primarily for improving the efficiency of lignocellulose delignification, xylan recovery for downstream enzymatic hydrolysis, and ethanol fermentation. Notably, the incorporation of a third component to conventional binary

Received: July 26, 2025

Revised: October 17, 2025

Accepted: October 21, 2025

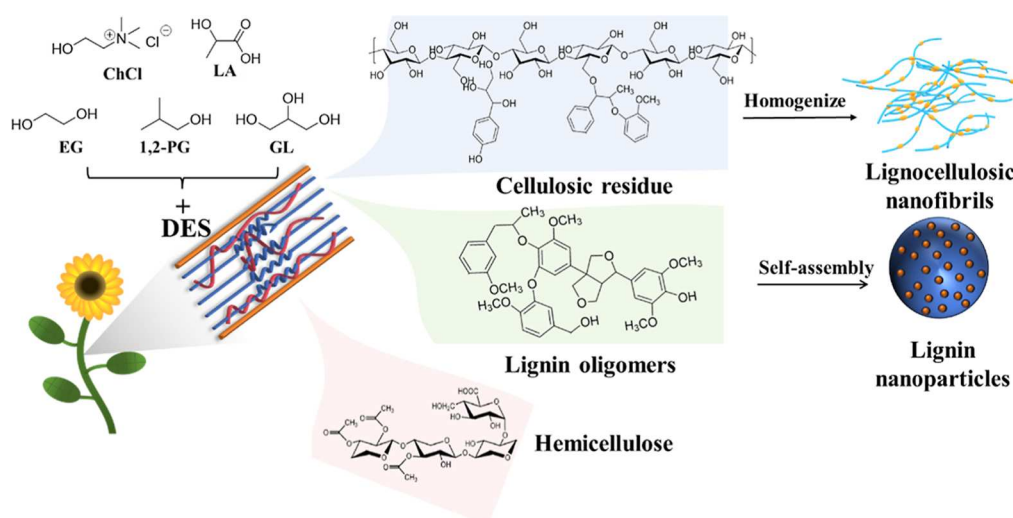


Figure 1. Schematic of the sunflower stalk fractionation process using bespoke ternary DES.

DES has been demonstrated to modify and improve the performance of acidic DES.¹³ This approach enhances mass transfer, reduces undesirable side reactions during pretreatment, and strengthens the comprehensive output.¹⁴ The combination of DES with organic and mineral acids (*p*-toluenesulfonic acid,¹⁵ salicylic acid,¹⁶ hydroxycarboxylic acids,¹⁷ hydroxyethyl sulfonic acid,¹⁸ and dilute sulfuric acid¹⁹) have shown to enhance the delignification efficiency. However, acid-comprising DES even under mild conditions induce undesirable side reactions, such as, lignin condensation, causing structural degradation, and restricting the downstream valorization of the extracted lignin.²⁰ Meanwhile, the incorporation of alcohols and polyols (e.g., ethylene glycol,²¹ ethanol,²² polyethylene glycol 200,²³ polyethylene glycol 400,²⁴ 1,3-propylene glycol,²⁵ and xylitol²⁶) and even water²⁷ has been reported to improve ethanol production via enhanced delignification. Jablonsky et al. demonstrated that the addition of alcohol as a third component decreased both the density and viscosity, thereby enhancing the delignification of various biomasses.¹¹ Similarly, Kandaneli et al. observed that alcohol supplementation improved the delignification efficiency by at least 50% relative to pure DES treatments.²⁸ Wang et al. further demonstrated that employing alcohol-based hydrogen bond donors (HBDs) increased the concentration of polar molecules, thereby enhancing microwave absorption capacity.²⁹ Yu et al. highlighted the effectiveness of diol-tailored DES in improving lignin fractionation, achieving yields up to 70%, whilst Poy et al. demonstrated the use of microwave-assisted ternary deep eutectic solvent pretreatment for improved rice straw saccharification as a mild pretreatment condition.³⁰

However, the combination of DES with polyols for the production of nanomaterials per se, specifically lignocellulosic nanofibrils (LCNFs) and lignin nanoparticles (LNPs), and the effects of polyols with different structural attributes (e.g., number and arrangement of hydroxyl groups) on the physicochemical properties of the resulting materials have rarely been investigated. This novel investigation provides insights into the synergistic mechanism of polyol-assisted ternary deep eutectic solvents to produce LCNFs and LNPs from sunflower stalks (Figure 1). Because the lactic acid (LA) and choline chloride (ChCl) binary DES system exhibits a relatively high delignification efficiency, we designed a series of

ternary DES by adjusting the molar ratios of the binary DES (lactic acid and choline chloride) and various polyols (glycerol, 1,2-propanediol, or ethylene glycol) (Table 1).

Table 1. Ternary DES Components

DES	HBA	HBD ₁	HBD ₂ (polyol s)	Molar ratio
CL12			/	1:2 1:2:1
CLE121			HO-CH ₂ -CH ₂ -OH	1:2:2
CLE122			EG	1:2:2
CLG121				1:2:1 1:2:2
CLG122				1:2:1 1:2:2
CLP121				1:2:1 1:2:2
CLP122				1:2:1 1:2:2

The role of these polyols in both the delignification efficiency and modulation of the physicochemical properties of the produced nanomaterials was systematically investigated. To the best of our knowledge, similar studies are still limited, and thus, this approach presents a promising direction for the sustainable and cost-effective production of nanomaterials with tunable properties from complex biomass resources.

2. MATERIALS AND METHODS

2.1. Materials. Sunflower cornstalks were obtained from the agricultural market in Tianjin, China, and dried (105 °C, 24 h until constant weight was achieved). The dried materials were ground (60-mesh grinder), subjected to Soxhlet extraction with ethanol for 4 h to remove lipids and waxes, and stored in airtight containers until further required. All chemicals used in the study, including lactic acid, choline chloride, 1,2-propanediol, ethylene glycol, glycerol, and ethanol, were analytically pure and purchased from Macklin (China). Deionized water was used throughout all experiments.

2.2. Synthesis and Characterization of Tailored Deep Eutectic Solvent. The components of the DES systems used in the experiments are summarized in Table 1. Prior to their synthesis,

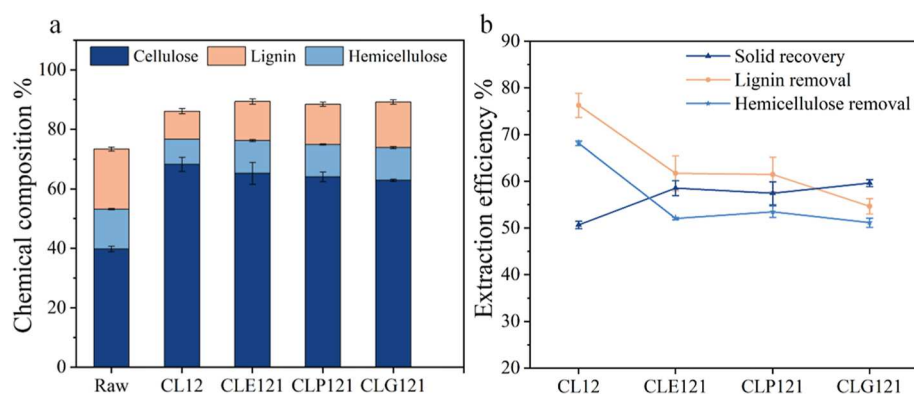


Figure 2. (a) Compositional analysis of raw materials and samples after DES pretreatment and (b) solid recovery, hemicellulose and lignin removal of samples.

choline chloride was dried in a vacuum oven at 80 °C for 6 h and then stored in a desiccator at room temperature. The tailored DES was synthesized by mixing choline chloride (ChCl), lactic acid (LA), and one of the polyols (glycerol, 1,2-propanediol, or ethylene glycol) in a round-bottom flask (250 mL) at specific molar ratios (1:2:1 and 1:2:2). The mixtures were then heated in a 250 mL round-bottom flask immersed in an oil bath at 80 °C with continuous stirring at 500 rpm until homogeneous transparent liquids formed. The resulting mixtures were cooled to room temperature in sealed vessels for further use. The DES samples were labeled CLE121, CLP121, CLG121, CLE122, CLP122, and CLG122, corresponding to the polyols used. The control group, comprising choline chloride and lactic acid (CL12), was prepared similarly. DES viscosity was measured with a viscometer (LiChen NDJ-79, China) at 100 °C with an appropriate speed of 1–200 rpm and the pH values of DES were determined using a pH meter (Shanghai Leizi PHS-3E, China).

2.3. Preparation of Lignocellulosic Nanofiber and Regenerated Lignin. The wax and lipid-free sunflower stalk powders were mixed with 50 mL of tailored DES at a ratio of 1:20 (w/v) in a flask, which was immersed in an oil bath and stirred magnetically at 130 °C for 9 h. Upon completion, the flask was cooled to room temperature using tap water, and the solid and liquid phases were separated via vacuum filtration. The solid residues were washed sequentially with hot water (30 mL, 60 °C) and ethanol (30 mL), each performed twice, followed by vacuum filtration and drying at room temperature for further characterization. LNPs were selectively recovered from the liquid phase by adding 400 mL of deionized water. The precipitated LNPs were then washed twice with a water/ethanol mixture (3:7 v/v) to remove residual DES, followed by centrifugation at 10,000 rpm for 5 min. The resulting LNPs were freeze-dried and stored in airtight glass vials for subsequent use. Both solid residues (LCNFs) and the recovered lignin nanoparticles (LNPs) were labeled based on the DES system used (e.g., CL12, CL121, and CL122).

The solid recovery, xylan removal efficiency, and delignification efficiency were calculated based on eqs 1–3, respectively

$$\text{solid recovery (\%)} = \frac{\text{sample after pretreatment}}{\text{raw material}} \times 100\% \quad (1)$$

$$\begin{aligned} \text{xylan removal (\%)} &= \frac{\% \text{ of xylan (raw material)} - \% \text{ of xylan (sample after pretreatment)}}{\% \text{ of xylan (raw material)}} \\ &\times 100\% \quad (2) \end{aligned}$$

$$\begin{aligned} \text{delignification efficiency} &= \frac{\% \text{ of lignin (raw material)} - \% \text{ of lignin (sample after pretreatment)}}{\% \text{ of lignin (raw material)}} \\ &\times 100\% \quad (3) \end{aligned}$$

2.4. Chemical Composition and Structure Analysis of Lignocellulosic Nanofibers and Lignin Nanoparticles.

2.4.1. Chemical Composition of Lignocellulosic Nanofibers. The chemical composition of LCNFs were determined according to the standard analytical National Renewable Energy Laboratory (NREL) protocol. Each sample underwent triplicate analyses to minimize the error.

2.4.2. Fourier Transform Infrared. Fourier transform infrared (FT-IR) spectra of LCNF and LNPs were recorded using a Thermo Scientific Nicolet iSTM5 FT-IR Spectrometer (Thermo Fisher Scientific, Waltham, MA, USA). Spectra were collected across a spectral range of 500–4000 cm^{-1} with a resolution of 2 cm^{-1} . The thermal decomposition properties of the samples were evaluated using a TG 209 F3 Tarsus thermogravimetric analyzer (Netzsch, Germany): samples (approximately 5–15 mg) were loaded into an alumina crucible and heated from room temperature to 650 °C for LCNFs and 800 °C for LNPs at a heating rate of 10 °C/min under a nitrogen flow of 20 mL/min. The first derivatives of the thermograms were calculated and smoothed with Origin 9.0.

2.4.3. X-ray Diffraction. XRD was performed using an Ultima-185 diffractometer (Rigaku, Rigaku, USA). The samples were conducted under Cu K α radiation ($\lambda = 1.5406 \text{ \AA}$) at 40 kV and 30 mA, with a scan speed of 10°/min and a scan range from 5 to 45 θ . Solid-state ^{13}C CP-MAS NMR spectra were obtained on a Bruker Avance NEO 400WB spectrometer (Germany); the spectra were collected by using a 4 mm CP-MAS probe with a sample spinning rate of 12 kHz and 64 scans. The crystallinity index (CrI) was calculated based on the integrated areas of the crystalline (86–92 ppm) and amorphous (80–86 ppm) regions using the following eq 4:³¹

$$\text{CrI} = \frac{A_{89-92\text{ppm}}}{A_{86-92\text{ppm}} + A_{80-86\text{ppm}}} \quad (4)$$

2.4.4. Two-Dimensional ^1H – ^{13}C Heteronuclear Signal Quantum Nuclear Magnetic Resonance. 2D HSQC NMR experiments were analyzed using a Bruker 400 MHz spectrometer (Germany) with ^1H (10–0 ppm) and ^{13}C (220–5 ppm) dimensions, respectively. The numbers of ^1H and ^{13}C data points were 1024 and 256, respectively, with a relaxation time of 1.5 s. The quantitative method based on 2D-HSQC spectra is shown in ES11.1.²⁵

2.4.5. Morphology Analysis. The morphologies and diameters of the samples were imaged using a MIRA LMS field-emission scanning electron microscope with an acceleration voltage of 3 kV (TESCAN, Czech Republic). Samples were placed on a copper shim, coated with gold, and mounted under liquid nitrogen conditions. The LNP diameters were statistically analyzed by measuring 100 randomly selected particles from SEM images using ImageJ software (NIH, USA). Transmission electron microscopy (TEM, JEM-F200) was also performed: a diluted LCNF suspension was gently deposited onto a copper grid and allowed to air-dry in a well-ventilated area. After imaging, the average diameters and diameter distributions of the LCNFs were determined by randomly measuring 100 fibers in the TEM images using ImageJ software.

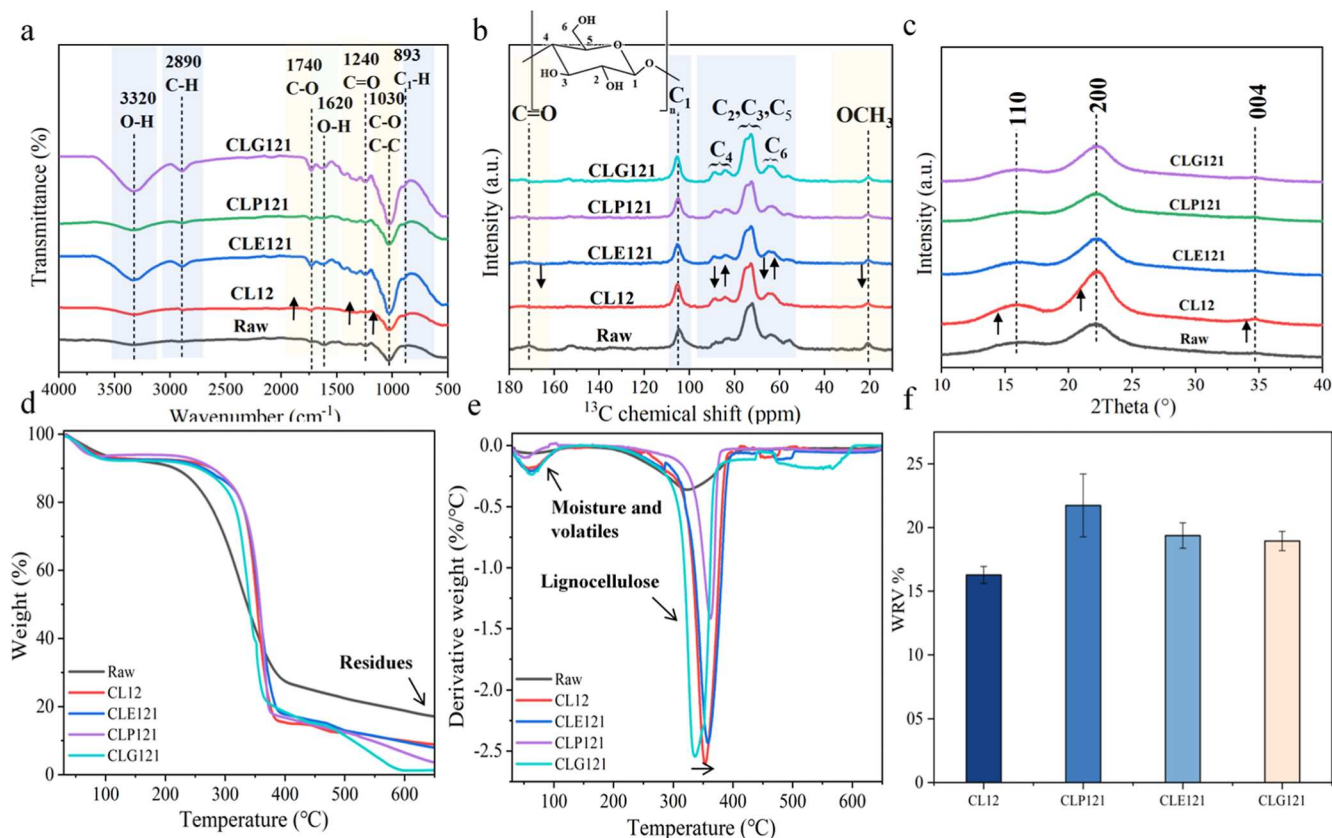


Figure 3. FTIR spectra (a), ¹³C CPMAS NMR spectra (b), and XRD diffractograms (c) of samples obtained from different DES systems. TGA thermograms (d), derivative thermogravimetric (DTG) profiles (e), and water retention value (WRV) (f) of the samples obtained from different DES systems ($N = 2$).

2.4.6. Zeta Potential and Water Retention Values. The zeta potentials of LCNFs and LNPs were conducted using a zeta potential analyzer (Nanobrook Omni, Brookhaven Instruments, USA). The appropriate samples were dispersed in deionized water with 0.1 wt % suspension and ultrasonicated for 15 min at 25 °C. The experiment was performed three times. The WRV was measured based on the SCAN-C 62:00 test method: a 2.5 wt %/v concentration of the slurry was centrifuged at 3000 rpm for 15 min and then dried (105 °C, 24 h). The WRV was calculated according to eq 5.

$$\text{WRV} = \frac{W_{\text{wet}} - W_{\text{dry}}}{W_{\text{dry}}} \quad (5)$$

2.4.7. GPC Analysis. The weight-average-molecular weight (M_w), number-average-molecular weight (M_n), and polydispersity index (PDI) of LNPs were determined by using a Thermo Scientific UltiMate 3000 gel permeation chromatography system (USA). Tetrahydrofuran (THF) was used as the mobile phase at a flow rate of 0.9 mL/min. The column and detector temperatures were maintained at 35 °C, with an injection volume of 40 μ L.

3. RESULTS AND DISCUSSION

3.1. Structural Characterization of Lignocellulosic Nanofibers. **3.1.1. Chemical Composition and Delignification Efficiency.** The chemical compositions of the samples are summarized in Figure 2 and Figure S1a. The results demonstrate that all DES pretreatments were effective for delignification: lignin was extracted into the DES, while varying degrees of hemicellulose degradation occurred. The delignification efficiency differs between the systems: the binary DES system achieved the highest delignification (76.28 \pm 2.6%), whereas polyol-assisted DES systems exhibit a relatively lower

efficiency (49.68 \pm 1.98–61.73 \pm 3.75%). Zhou et al. reported the delignification efficiency of wheat straw using polyol-assisted acidic DES pretreatment for improving enzymatic hydrolysis of wheat straw 54.1 \pm 0.3% (binary) and 73.5 \pm 1.4% (ternary).¹³ Our binary DES system achieved the highest delignification (76.28 \pm 2.6%), whereas the polyol-assisted DES ternary systems exhibit a relatively lower efficiency (49.68 \pm 1.98–61.73 \pm 3.75%). These results contrast with previous reports, albeit in the wheat straw (binary 54.1 \pm 0.3% vs ternary 73.5 \pm 1.4%),¹³ most likely since the acidity and viscosity of the DES significantly influences the efficiency of pretreatment.³² Specifically, a high acidity (α) value of the DES enables the efficient donation and release of H⁺, thereby promoting the cleavage of β -O-4 ether linkages and hydrogen bonds in the lignin-carbohydrate complexes, leading to greater delignification. Although polyol incorporation reduced the DES viscosity (see ESI Figure S2), it concurrently diminished the solvent acidity (see ESI Figure S3), thus lowering the lignin dissolution and hemicellulose degradation efficiency. Interestingly, the raw materials display a lower content of the composition as compared to that of the treated samples; this is possibly due to the fact that no-lignocellulosic matter (e.g., inorganic salts) was also isolated during DES pretreatment.

The effect of polyols with various numbers of hydroxyl groups was also assessed. DES-containing polyols with a higher number of hydroxyl groups (e.g., CLG122) showed the lowest delignification and hemicellulose removal (49.68 \pm 1.98% and 41.72 \pm 2.78%, Figure S1b). This may be attributed to polyols with a greater number of hydroxyl groups tending to form stronger intermolecular hydrogen bonds with the Cl⁻ ions in

the choline chloride component of the DES. The increased hydrogen bonding within the DES reduces its ability to interact effectively with lignin, thereby weakening the pretreatment efficiency.¹³ Meanwhile, increasing the molar ratio of ChCl/LA/polyol from 1:2:1 to 1:2:2 resulted in an inferior delignification efficiency (Figure S1b), indicating that higher amounts of polyols are negatively associated with lignin removal. These findings are consistent with the compositional data, for example, NMR, XRD, and TGA, reported later. Thus, incorporating polyols into the DES allows the tuning of delignification efficiency during pretreatment. This is beneficial for future preparations of LCNF with an adjustable lignin content. Notably, 10.85–11.99% of xylan was retained after polyol-assisted DES treatment, significantly higher than the 8.42% retention observed with binary DES pretreatment (CL12). These results demonstrate that polyol-assisted DES inhibits excessive hemicellulose degradation and selectively cleaves the C–O bonds of lignin–carbohydrate complexes, thereby exhibiting outstanding selectivity for lignin removal and xylan retention. This is consistent with Li's research.³³ Such selective preservation of xylan is advantageous for subsequent downstream enzymatic hydrolysis and ethanol fermentation processes. In summary, incorporating polyols into the DES allows for the selective tailoring of the LCNF composition while conserving essential carbohydrate components during lignocellulose pretreatment, the solid recovery and crystallinity index (CrI, determined by ¹³C CPMAS spectroscopy, see Figure S4) of the samples obtained from various DES systems are presented in Figures 2 and S1b. The LCNFs treated with binary DES exhibit the lowest yield (50.68%) compared to samples treated with polyol-assisted DES systems, which range from 57.46 to 66.51%. A positive correlation is observed between the polyol ratio (1:2:1–1:2:2) and the yield (57.46–66.51%), with CLG122 exhibiting the highest yield (66.51%). In contrast, the CrI of LCNFs decreases with an increasing polyol ratio (40.98–36.36%), indicating that the higher acidity of the binary DES facilitated a more extensive removal of hemicellulose and lignin from the lignocellulosic matrix during pretreatment.

3.1.2. Fourier Transform Infrared Analysis. FT-IR spectroscopy was used to evaluate changes in the primary functional groups of LCNFs following DES treatment, and the spectra of the samples obtained in this study are shown in Figure 3a. The absorbance bands observed around 3320 cm⁻¹ correspond to the O–H stretching vibration; the intensity of these signals increases, indicating that cellulose exposes more hydroxyl groups during DES treatment. The absorbance band near 2890 cm⁻¹ is attributed to the C–H stretching in the carbohydrate backbone.³⁴ The absorption band at approximately 1740 cm⁻¹ is associated with carbonyl groups from residual hemicellulose and lignin,³⁵ and the vibration at 1240 cm⁻¹ corresponds to C–O stretching in xyloglucan (hemicellulose), the bands around 1030 cm⁻¹ are the C–O stretching of methoxy groups of the guaiacyl unit (G) in lignin. Notably, the intensities of these three bands increase upon the introduction of polyols into the DES, indicating the partial removal of lignin and hemicellulose. This is consistent with Zhou et al. and is attributable to increased hydrogen bonding within the DES, which limits the formation of effective interactions with lignin and, thus, weakening the removal of hemicellulose and lignin.¹³ The bending vibration around 1620 cm⁻¹ may correspond to bound water present in the LCNFs. Finally, the bands at 893 cm⁻¹ refer to the C₁–H

deformation of the glucose ring, and a slight increase in the intensity of the peaks after DES treatment indicates a higher purity of the polyol in DES, indicating the reduced removal of hemicellulose and lignin. Overall, the disappearance of these noncellulosic components highlights the effectiveness of ternary DES pretreatment and confirms the cellulose as the primary component.

3.1.3. Solid-State ¹³C CPMAS NMR. The FT-IR findings are further supported by ¹³C CPMAS NMR spectra (Figure 3b), which illustrate the structural changes in LCNFs following the treatment with various DES systems. The resonance at 175 ppm is attributed to the carbonyl/carboxylic groups in hemicelluloses present in the sunflower stalk cell wall, while the low-intensity peak at 153 ppm corresponds to oxygenated aromatic carbons in lignin.³⁶ The region between 110 and 60 ppm covers the characteristic cellulose carbon signals (C₁–C₆),³⁷ and the resonance at 20 ppm originates from the acetyl group in the hemicellulose. After DES treatment, the intensities of the signals assigned to the hemicellulose and lignin decrease markedly, especially in CL12 samples, indicating the enhanced cleavage and removal of these components in the binary DES system. Furthermore, changes in the cellulose structure are also observed: the ratio of cellulosic surface/amorphous carbons at C₄ and C₆ (84 and 62 ppm, respectively) decreased, while the interior/crystalline carbons at C₄ and C₆ (89 and 65 ppm, respectively) increased. This suggests that the amorphous regions of the cellulose were gradually hydrolyzed during DES treatment, while the crystalline regions remained intact.³⁸ This trend is consistent with previous findings.³⁴

3.1.4. X-ray Powder Diffraction Analysis. The crystallinity of LCNF is a critical parameter influencing their biodegradability, thermal stability, and mechanical properties. X-ray diffraction (XRD) analysis was conducted to assess the crystalline structure of LCNFs, with patterns for both untreated and treated samples presented in Figure 3c. All samples exhibited distinct cellulose characteristic peaks at 2θ values of 16.5°, 22.5°, and 34.5°, corresponding to the Miller indices (110), (200), and (004), respectively, indicating that the crystalline structure of the cellulose was preserved during DES processing.³⁹ After treatment, these crystalline peaks increased and became more pronounced, reflecting the progressive removal of amorphous polysaccharides (such as hemicellulose and amorphous cellulose) and lignin. Notably, samples treated with binary DES (CL12) exhibited the most pronounced crystalline peaks, indicating more extensive removal of amorphous cellulose, hemicellulose, and lignin compared to that of ternary DES treatments. As reported by Zhou et al.,¹³ this is attributed to the higher acidity and delignification efficiency of the binary system, whereas increasing the polyol content reduces DES acidity and limits delignification. Furthermore, as the CrI of samples are positively correlated with the delignification efficiency, increasing polyol content in the ternary DES system (from a molar ratio of ChCl/LA/polyols of 1:2:1 to 1:2:2) also resulted in decreased CrI values for LCNFs, indicating the preservation of amorphous polysaccharides—consistent with FT-IR and NMR results.

3.1.5. Thermal Analysis. Thermogravimetric (TG) and derivative thermogravimetric (DTG) analyses were performed to evaluate the thermal decomposition behavior and composition of LCNFs, with the curves presented in Figure 3d,e. Moisture and volatile compounds constitute 6–10 wt %

of the samples, while the lignocellulose accounted for approximately 80 wt % of the total mass. Untreated samples exhibited a higher residue content (21%) compared to LCNFs (2–15% for CL, CLE, CLG, and CLP), likely due to the removal of inorganic minerals during DES processing. The DTG curves revealed three primary degradation stages: (i) the initial degradation temperature of the samples is approximately 30–110 °C, attributed to the loss of moisture/volatiles (6–10%); (ii) the main band at around 240–330 °C is attributed to hemicellulose decomposition, and this band is only clearly observed in the untreated sample, indicating that most hemicellulose was removed during DES treatment, and (iii) the band at 340–380 °C is associated with cellulose decomposition. Interestingly, the DTG peaks for most DES-treated samples shift to higher temperatures (348.18–363.94 °C) compared to untreated samples (323.94 °C), suggesting the removal of amorphous cellulose and hemicellulose during the DES treatment and the stability of the cellulose increased due to enhanced crystallinity.^{34,40} These results are in agreement with the crystallinity changes indicated by XRD and solid-state NMR analyses.

3.1.6. Water Retention Value. As presented in Figure 3f, the samples treated with polyol-assisted DES generally exhibited higher WRV (16.4–21.7%) compared to those treated with the binary DES system (CL12, 16.3%), this enhancement is attributed to the swelling properties facilitated by polyols, which likely improve DES penetration into the biomass structure and subsequently increase the water absorption capacity of the insoluble LCNFs within the fibril network.⁴¹ Additionally, the presence of polyols might mitigate lignin condensation onto the cellulose surface, further contributing to the improved water-holding capacity of LCNFs, an interpretation supported by SEM observations (Figure S5). The enhanced water retention of LCNFs makes them suitable for applications such as hydrogels and biobased rheology modifiers in various sectors such as pharmaceuticals and home and personal care.

3.1.7. Zeta Potential. The zeta potential, which reflects the surface charge and colloidal stability of LCNF suspensions, was determined for samples obtained from different DES treatments (Table 2). Due to the presence of numerous hydroxyl

Table 2. Zeta Potential (mV) of LCNFs Obtained from Different DES

LCNF	zeta potential (mV)
CL12	-21.94 ± 2.31
CLE121	-25.24 ± 1.65
CLP121	-21.10 ± 3.26
CLG121	-32.93 ± 0.01

groups on the cellulose, all LCNF aqueous suspensions exhibited negative zeta potential values, ranging from -21.94 to -32.93 mV.⁴² Previous research has demonstrated that LCNF suspensions with an absolute zeta potential value greater than 15 mV exhibited a stronger stability. This suggests that the LCNF suspensions prepared through the DES pretreatment exhibit good stability. Notably, the zeta potential of LCNFs treated with CLE121 and CLG121 systems is more negative compared to those treated with the CL12 system. This could be attributed to the presence of negatively charged lignin structures on the LCNF surface, enhancing electrostatic repulsion between fibrils, thus counteracting agglomeration

tendencies and contributing to a higher overall negative charge.⁴⁴ Conversely, LCNFs processed with the CLP121 system display lower zeta potential values than those derived from CL12, likely due to the larger particle sizes observed in CLP121 samples, which result in a reduced surface charge density and subsequently less negative zeta potential values.

3.1.8. Morphology: Scanning Electron Microscopy and Transmission Electron Microscopy. Scanning electron microscopy (SEM) images reveal surface morphological changes in lignocellulosic residues after DES processing (Figure S5). Untreated fibers displayed a highly dense and smooth structure, whereas DES-treated samples fragmented into independent fiber bundles with slightly damaged structures and porous surfaces. Meanwhile, with the introduction of polyols, the surface roughness of LCNFs was reduced, which is attributed to the reduced acidity of the DES resulting from the incorporation of polyols.¹³ These morphological alterations are primarily attributed to the cleavage of ether (C–O) linkages within the lignocellulosic matrix during the DES treatment, resulting in the substantial removal of lignocellulosic components, such as amorphous cellulose, hemicellulose, and lignin, thereby disrupting the original tissue network integrity. These morphological changes correlate well with the WRV and crystallinity index data reported earlier and Zhou et al.'s reports.¹³

Transmission electron microscopy (TEM) was also employed to further investigate the LCNF morphology and measure fiber diameters, as illustrated in Figures 4 and S6. The TEM images demonstrate that the LCNFs exhibit nanoscale dimensions with good dispersibility, indicating the effective removal of noncellulosic components from the sunflower stalks during pretreatment. Meanwhile, the robust hydrogen-bond network between cellulose chains was also disrupted, resulting in the dissociation of the network into slender interwoven nanofibers. The presence of dark particles corresponds to the residual lignin that was not entirely removed. The LCNFs exhibit uniform widths ranging from 13.46 to 18.84 nm, suggesting successful DES pretreatment and homogenization in deconstructing the raw material for efficient nanofiber production (Figure S6). All LCNFs treated with polyol-assisted DES systems exhibited diameters larger than those treated with CL12, likely due to the higher acidity of CL12, which induces more pronounced lignocellulose hydrolysis. In contrast, LCNFs derived from the CLE122 treatment displayed the smallest average diameters among the samples (13.46 nm, Figure S5j), this is possibly due to the enhanced swelling effect of ethylene glycol on the cellulose structure, which could promote finer fibrillation during homogenization. Overall, the successful isolation of LCNFs with small diameters and relatively narrow size distributions highlights their potential suitability for advanced applications, such as drug carriers and reinforcing agents.

3.2. Structural Characterization and Comparison of Lignin Nanoparticles. To gain more insights into the fundamental structural characteristics (unit connectivity and unit types) of the regenerated lignin fractions after DES treatment, 2D HSQC NMR, GPC, and FTIR spectroscopy was performed to detect their elaborate chemical compositions.

3.2.1. Fourier Transform Infrared Analysis. To investigate the functional group changes in LNPs derived from various DES systems, FT-IR spectroscopy was employed, and the resulting spectra are displayed in Figure 5a,b. All samples exhibited similar profiles, indicating comparable structural

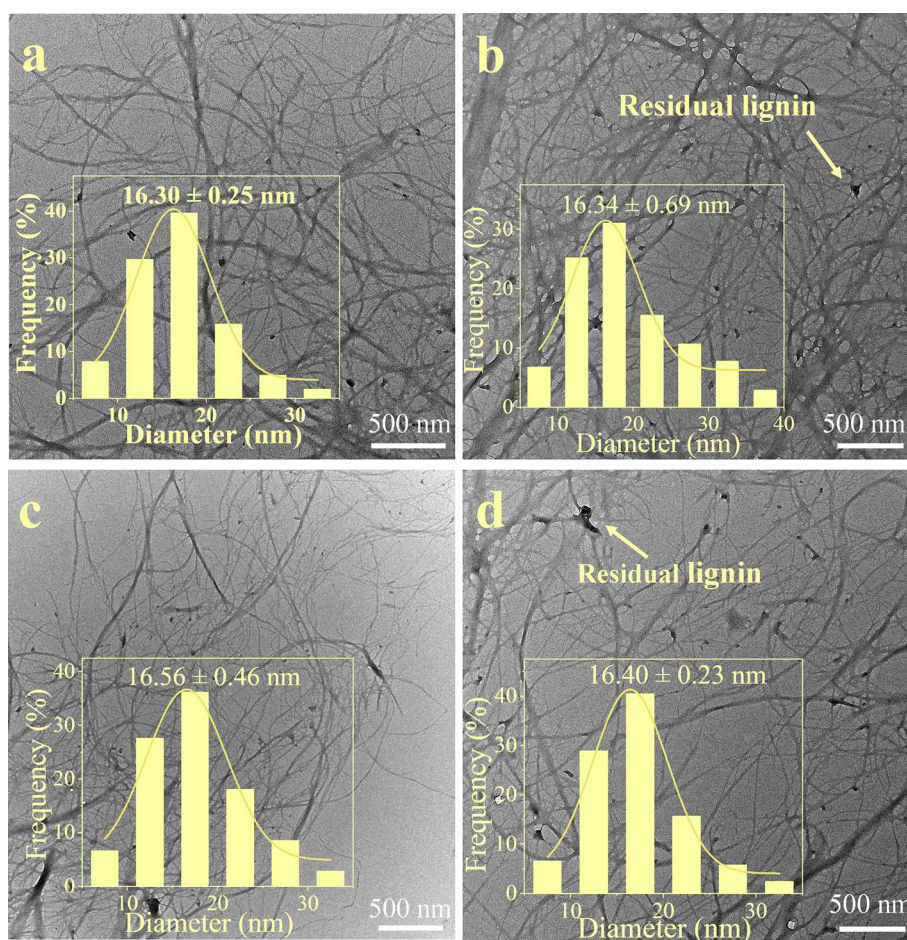


Figure 4. TEM images and particle size distributions of LCNFs prepared from CL12 (a), CLE121 (b), CLP121 (c), and CLG121 (d).

features. The band at 3420 cm^{-1} corresponds to the stretching vibration of aliphatic and phenolic hydroxyl groups, while the peak at 2940 cm^{-1} is attributed to the C–H stretching of methyl and methylene groups. The absorption band around 1730 cm^{-1} is indicative of carbonyl groups, confirming the presence of lignin. Upon the introduction of polyols during DES treatment, an increase in the absorption intensities of the C–O bands was observed, suggesting a reduced cleavage of C–O bonds. The peaks at 1600 cm^{-1} are C=C stretching vibrations in the benzene ring of lignin. The bands at 1510 cm^{-1} and 1460 cm^{-1} correspond to the vibrations of the aromatic skeleton, confirming the existence of aromatic ring structures in lignin.⁴⁵ No significant changes had occurred indicating that the aromatic skeleton of LNPs was well retained during processing.⁴⁶ The peak at 1220 cm^{-1} is assigned to C–O stretching vibrations of phenolic hydroxyl and phenolic ether groups, while the band at 1120 cm^{-1} corresponds to the aromatic C–H in-plane deformation of the syringyl unit(S). Additionally, the signal at approximately 1030 cm^{-1} may attribute to the C–O stretch of methoxy groups of the guaiacyl unit (G) in lignin, indicating that the LNPs are of the G-S type.⁴⁷ These results are consistent with the 2D-HSQC NMR data (see later). All samples retained the structural characteristics of phenolic hydroxyl and C–O bonds, demonstrating that their structures remained highly similar even when polyols were introduced into the binary DES system. This is consistent with the findings of Li et al.³³ Notably, the characteristic signals corresponding to the hemicellulose, such as those

around 1240 cm^{-1} , were not clearly observed, suggesting that the LNPs possess a relatively high purity during DES pretreatment, which is favorable for further valorization.

3.2.2. Thermal Analysis. To evaluate the thermal stability of LNPs, thermogravimetric analysis (TGA) and their derivative thermogravimetry (DTG) were performed, with the corresponding curves displayed in Figure 5c,d. Three distinct mass loss stages were identified: (i) a minor mass loss of approximately 7% was observed, attributed to the evaporation of moisture and low-molecular-weight volatiles present in the sample; (ii) the most significant mass loss ($\sim 38\%$) is due to the thermal cleavage of broken of C–O and aryl ether (β -O-4, α -O-4, and 4-O-5) bonds between lignin structural units.¹⁵ During this phase, lignin partially decomposed into tar and combustible gases, such as CH_4 , CO , and CO_2 , and (iii) between 500 and $700\text{ }^\circ\text{C}$, the rate of mass loss progressively declined due to advanced depolymerization and carbonization processes within the lignin macromolecular structure. Among the tested samples, LNPs derived from binary DES treatments showed the highest char yield (43.1%) and superior thermal stability, with a maximum degradation temperature of $366.4\text{ }^\circ\text{C}$. However, the samples treated with polyol-assisted DES systems exhibited elevated carbon residues ranging from 35 to 44% and thermal stability. This enhancement in thermal stability may be attributed to a higher degree of C–C linkage formation in CL12 samples during treatment, leading to reduced pyrolytic reactivity and a more condensed structure, which is consistent with Zhai et al.'s work who reported that

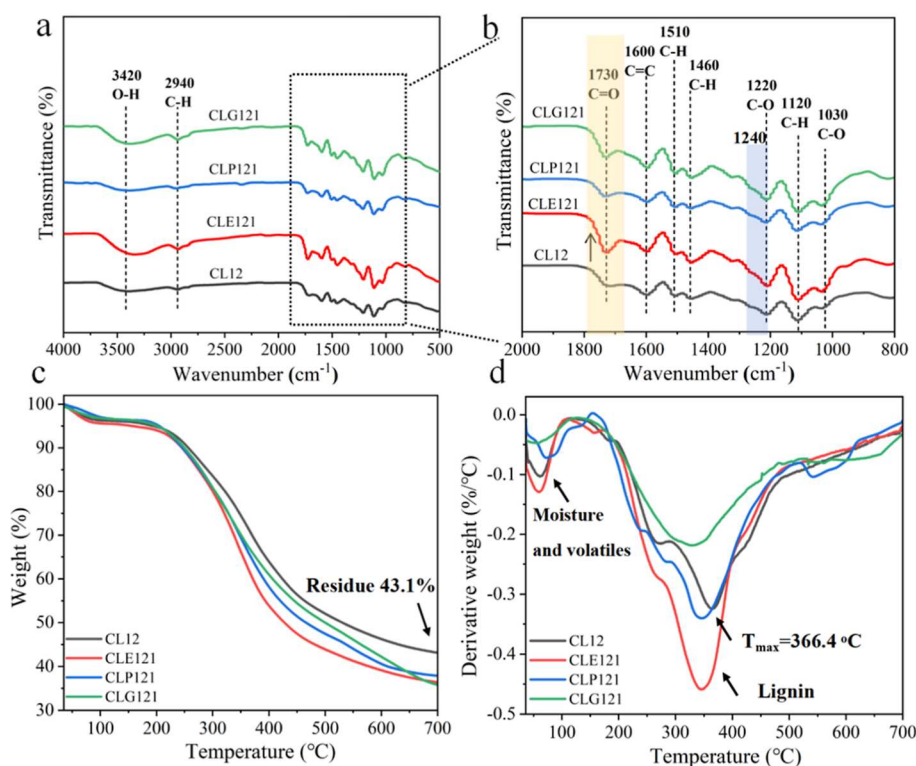


Figure 5. FT-IR (a) and partially enlarged IR spectral (b) of LNPs obtained from different DES systems. TGA thermograms (c) and DTG profiles (d) of LNPs obtained from different DES systems.

the decomposition temperature increased with increased treatment severity.¹⁵ The observation is supported by 2D-HSQC NMR analysis, which revealed a greater extent of condensation and structural integrity in these samples.

3.2.3. 2D-HSQC NMR Analysis of Lignin Nanoparticles. To investigate the detailed structural characteristics of the regenerated lignin nanoparticles extracted from sunflower stalks using DES, 2D HSQC NMR was performed, and the predominant substructures of the lignin are identified and are presented in Figure 6. In the side-chain region (δ_C/δ_H 50–90/2.5–6.0 ppm), a prominent correlation at δ_C/δ_H 56.54/3.70 ppm corresponds to methoxy groups ($-\text{OCH}_3$), indicated a high content of syringyl (S) and guaiacyl (G) units in the lignin fractions, which is consistent with FT-IR spectra. The major interunit linkages identified in samples are β -O-4 ether bonds (A) and resinol-type β - β bonds (B), which are typical in lignin macromolecules. The signals corresponding to the β -O-4 linkages are detected at δ_C/δ_H 72.6/4.82 ppm (α -position), 81.8/4.51–4.64 ppm (β -position), and 60.6/3.12–4.03 ppm or 66.3/4.04 ppm (γ -position), respectively.⁴⁶ For resinol-type (β - β , B) linkages, characteristic peaks were observed at δ_C/δ_H 85.8/4.62 ppm (B_α), 54.1/3.14 ppm (B_β), and 71.6/3.62–4.24 ppm (B_γ).⁴⁸ Additionally, signals at δ_C/δ_H 87.8/5.47 and 67.1/3.42–3.93 ppm are attributed to the α and γ positions of the resinol (C) structure.⁴⁹ Finally, the lactic acid signals for L_2 at δ_C/δ_H 69.1/4.9 ppm are also detected. The results reveal that many functional groups of LNPs were retained, indicating that the lignin structure was well preserved during DES extraction and nanoparticle formation. As the high content of β -O-4' linkages in lignin fractions relate to high quality and being less condensed which has great promise for subsequent valorisation,⁵⁰ the relative abundance of interunit linkages was semiquantitatively determined by the volume

integration of 2D HSQC NMR spectra. The LNPs obtained from the polyol-assisted DES system contained a higher proportion of β -O-4' linkages compared to those from conventional LNP (CL12) samples (ESI Table S1), indicating the better preservation of the native lignin structure.⁵¹

In the aromatic region (δ_C/δ_H 100–135/5.5–9.0 ppm), the HSQC spectra revealed that guaiacyl (G) and syringyl units (S) are the predominant aromatic components of the regenerated lignin from sunflower stalks, as shown in Figure 6a–d. Characteristic signals for the guaiacyl unit (G) are observed at δ_C/δ_H 111.3/6.94 (G_2), 115.7/6.75 (G_5), and 119.7/6.78 (G_6), respectively. The signals of syringyl units (S) are detected at δ_C/δ_H 103.9/6.61 ($S_{2,6}$).⁵² Signals corresponding to condensed syringyl units (S) appear at δ_C/δ_H = 106.1/6.45. Semiquantitative analysis shows that the relative intensity of these condensation signals decreased from 21.8% in CL12 to 10.3% in the polyol-assisted DES-treated samples (ESI Table S1). This significant reduction can be explained by the fact that β -O-4' linkages are acid sensitivity and prone to form benzyl carbocations, normally causing condensation under acidic conditions.⁵³ The incorporation of polyols can react with carbocation intermediates and forming the α -etherified lignin, which stabilizes the lignin structure, thereby reducing condensation reactions and degradation of the lignin, leading to the extraction of high-quality less-condensed lignin, which is consistent with previous reports.²⁰ The possible reaction pathways is presented in Figure S7.⁵¹

3.2.4. Molecular Weight Distribution of Lignin Nanoparticles. To investigate the depolymerization behavior of LNPs derived from various DES systems, the M_w , M_n , and PDI are determined by GPC and are summarized in Tables 3 and S2. All LNP samples exhibited molecular weight distributions in the range of 1450–2676 g/mol, which are lower compared

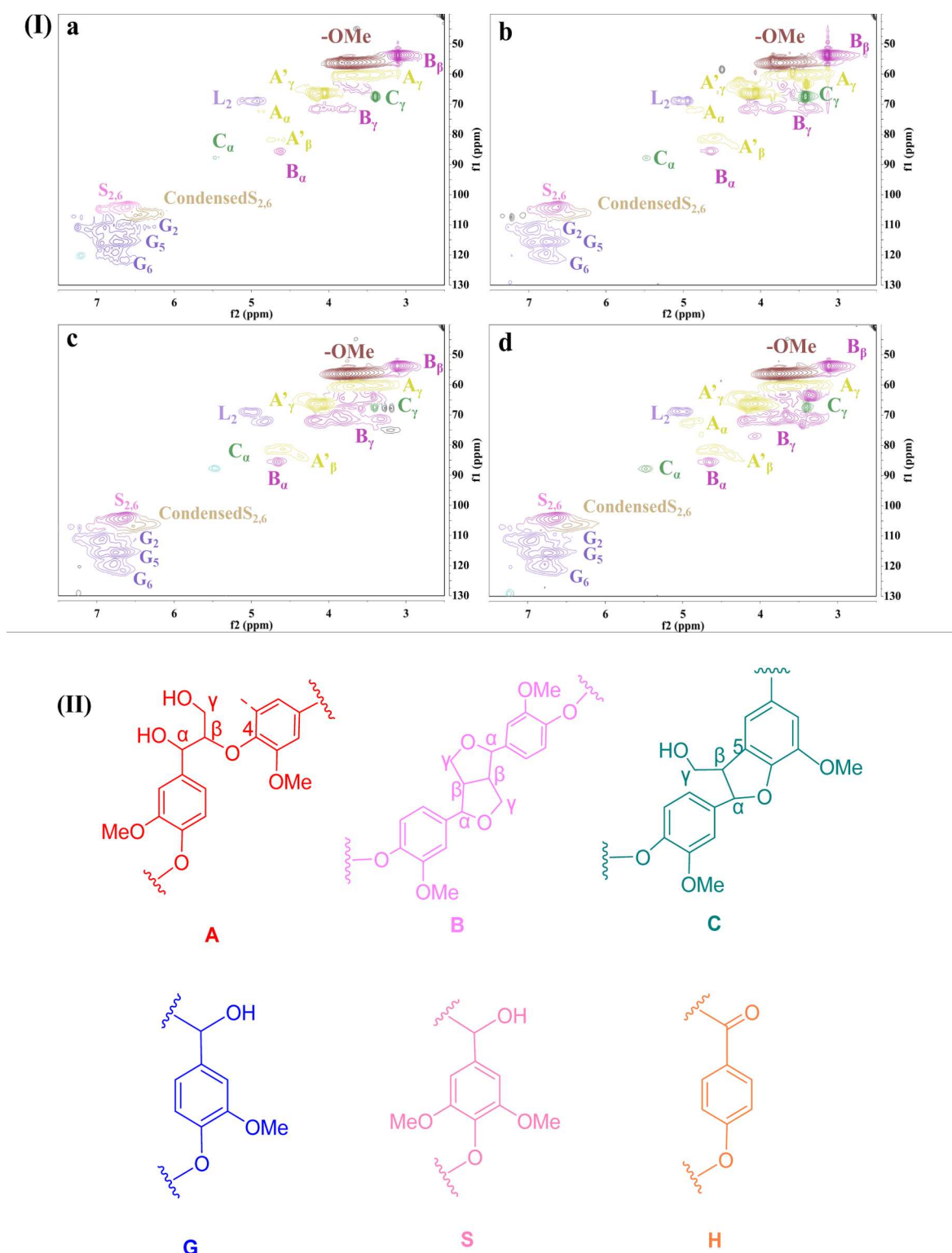


Figure 6. (I) The aliphatic regions and aromatic regions in 2D HSQC spectra of LNPs obtained from CL12 (a), CLE121 (b), CLP121 (c), CLG121 (d); and (II) their substructures, aryl ether (A), resinol-type β - β bonds (B), resinol (C), guaiacyl (G), syringyl (S), and lactic acid (L_2).

with previous studies (2923–7232 g/mol).⁴³ This may be due to the milder conditions (DES plus polyol) retaining a lower molecular weight lignin with a narrow distribution compared with the more aggressive DES plus *p*-toluenesulfonic acid, which cleaves indiscriminately affording a wider distribution. LNPs obtained from polyol-assisted DES systems exhibited higher M_w values ranging from 1838 to 2676 g/mol and M_n

values from 1102 to 2054 g/mol. This suggests that the molecular weight is closely related to the extent of the β -O-4 bond cleavage by DES, polyols are believed to stabilize benzyl carbocations, thereby suppressing condensation reactions and preserving the integrity of the lignin structure. Consequently, the LNPs extracted using ternary DES systems were more homogeneous and structurally complete, consistent with

Table 3. The Molecular Weight Distribution and polydispersity index (PDI) of LNPs Obtained from Different DES Systems

LNP	M_w	M_n	PDI
CL	1450	947	1.53
CLE121	2508	1994	1.26
CLP121	1838	1102	1.67
CLG121	2417	1986	1.22

previous findings.⁴⁶ The PDI values (M_w/M_n) of all samples range from 1.22 to 1.67, which are below 2, indicating a relatively narrow molecular weight distribution.⁵⁴ These lower values of PDI support the suitability of these LNPs for the production of high-value added chemicals. As PDI values are negatively associated with lignin condensation, it is found that the PDI decreased with the incorporation of polyols, indicating that LNPs treated with polyol-assisted DES represent a lower condensation; the results are in agreement with 2D-HSQC NMR data above.

3.2.5. Stability of Lignin Nanoparticles (Zeta Potential). The zeta potentials of various LNP samples are summarized in Tables 4 and S3. Due to the deprotonation of acidic functional

Table 4. The Zeta Potential (mV) and Average Diameter (nm) of LNPs Obtained from Different DES Systems

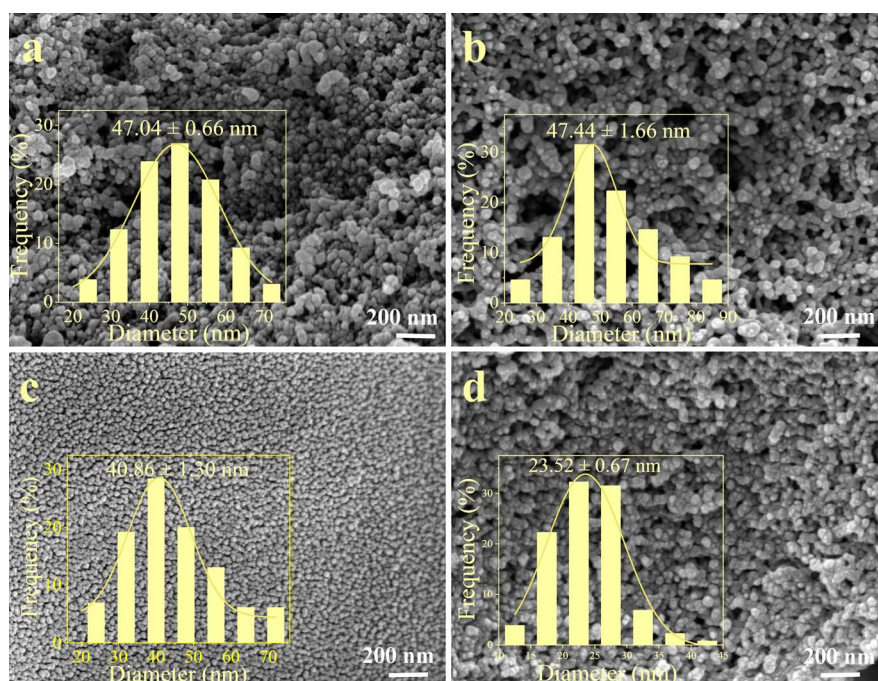
LNPs	average diameter (nm)	zeta potential (mV)
CL	47.04 ± 0.66	-24.9 ± 5.1
CLE121	47.44 ± 1.66	-28.1 ± 3.9
CLP121	23.52 ± 0.67	-25.6 ± 0.5
CLG121	40.86 ± 1.30	-27.3 ± 1.1

groups (e.g., carboxyl and phenolic hydroxyl groups) on the lignin backbone, all samples exhibited negative surface charges, consistent with the findings in previous studies.⁵⁵ Among all of the samples, CLE121 displayed the most negative zeta

potential (-28.1 ± 3.9 mV), followed by CLG121 (-27.3 ± 1.1 mV), CLP121 (-25.6 ± 0.5 mV), and the conventional LNP sample obtained from CL12 (-24.9 ± 5.1 mV). The results are consistent with those in the literature. For example, the zeta potential of lignin nanoparticles derived from fractionation using water plus ethanol or GVL as a cosolvent range from -14.9 ± 1.4 to 39.6 ± 1.0 mV.⁴⁰ Generally, a higher negative zeta potential indicates stronger electrostatic repulsion between particles, which minimizes aggregation and leads to smaller average particle sizes. The increase in the zeta potential upon the addition of polyols during DES treatment suggests that polyols can enhance particle stability and size control. The reason may be the fact that the introduction of polyols inhibits the condensation of lignin via carbocation capture to form α -alkoxylated lignin.²⁵

Overall, all samples tend to form small lignin particles with a spherical structure and narrow range of size distribution. These findings imply that by modulating polyol ratio and types in DES systems, it may become a crucial part in fine-tuning the size and dispersion characteristics of LNPs for targeted applications.

3.2.6. Morphology of Lignin Nanoparticles. The morphological features of the prepared LNPs are shown in Figures 7 and S8. All samples exhibited a spherical morphology with a narrow nanoscale size distribution, suggesting that the LNPs were formed through the self-assembly of extracted lignin fragments.⁵⁶ This confirms the feasibility of producing well-defined LNPs using polyol-assisted DES systems in a simplified and tailored process. CLG121 produced the smallest average particle size at approximately 24 nm, while CLP122 displayed the largest average size at about 66 nm. Notably, LNPs derived from polyol-assisted DES systems generally exhibit smaller particle sizes than those from CL12, this may be attributed to lower hydrophilicity from the binary DES system facilitated the formation of LNPs with a smaller size,⁵⁷ highlighting the beneficial role of polyols in facilitating nanoparticle formation.

**Figure 7.** SEM images and particle size distributions of LNPs prepared from CL12 (a), CLE121 (b), CLP121 (c), and CLG121 (d).

However, with the increasing polyol content in the DES formulation, the particle size tended to increase; this is hypothesized to the stabilization and solubility of lignin macromolecules being effectively enhanced by polyol, which minimizes lignin fragmentation and facilitates the formation of larger self-assembled structures.

4. CONCLUSIONS

In our global quest for sustainability and sustainable development, the increasing use of lignocellulosic, nonfood competing, renewable resources, and their fractionation into the cellulose, hemicellulose, and lignin for further downstream processing into platform chemicals, functional materials, and bioenergy within the context of biorefineries is critical. Where best, such biorefineries will operate using benign processes. For example, tuning the relative ratios of polyols in DES systems to fractionate sunflower stalks into lignocellulosic fibers and lignin nanoparticles opens a promising approach for biobased industrial applications and provides a feasible path for sustainable development.

The integration of polyols into choline chloride/lactic acid DES systems allows for the precise control of LCNF and LNP properties. However, the addition of polyol leads to a decrease in the delignification efficiency, effectively inhibiting the excessive degradation of the hemicellulose. Polyol-assisted DES pretreatment achieves the controlled lignin content in LCNFs (49.68–76.28%), reduced a degree of condensation (10.3% vs 21.8% in control), and molecular weight ranges (1838–2676 g/mol) that allow for easy processability with preserved β -O-4 linkages in LNPs through carbocation stabilization. These findings clearly demonstrate that polyols play a crucial role in protecting β -O-4 linkages and inhibit lignin condensation during pretreatment, which is a critical enabler for processability and wider applications of lignin as a biobased material.

■ ASSOCIATED CONTENT

SI Supporting Information

The Supporting Information is available free of charge at <https://pubs.acs.org/doi/10.1021/acssuschemeng.5c07767>.

Compositional analysis; removal efficiency; viscosity and pH of DES; CrI and SEM images of LCNFs; molecular weight distribution, zeta potential, and average diameter of LNPs (PDF)

■ AUTHOR INFORMATION

Corresponding Authors

Yang Gao – State Key Laboratory of Separation Membrane and Membrane Process, School of Chemistry, Tiangong University, Tianjin 300387, PR China; Email: yg1042@tiangong.edu.cn

Shichao Xu – School of Environmental Science and Engineering, Tiangong University, Tianjin 300387, PR China; Email: xushichao@tiangong.edu.cn

Avtar S. Matharu – Green Chemistry Centre of Excellence, Department of Chemistry, University of York, York YO10 SDD, U.K.; orcid.org/0000-0002-9488-565X; Email: avtar.matharu@york.ac.uk

Authors

Ruipeng Ji – State Key Laboratory of Separation Membrane and Membrane Process, School of Chemistry, Tiangong

University, Tianjin 300387, PR China; orcid.org/0009-0000-8795-7152

Ziyi Ren – State Key Laboratory of Separation Membrane and Membrane Process, School of Chemistry, Tiangong University, Tianjin 300387, PR China

Zhicheng Jiang – College of Biomass Science and Engineering, Sichuan University, Chengdu 610065, PR China; orcid.org/0000-0002-8096-4971

Complete contact information is available at:

<https://pubs.acs.org/10.1021/acssuschemeng.5c07767>

Author Contributions

Y.G.: writing, conceptualization, original draft, review and editing, funding acquisition. R.J.: writing—formal analysis, data curation. Z.R.: figures. Z.J.: figures. S.X.: review & editing. A.S.M.: initial research and ongoing discussions with Y.G. review & editing.

Notes

The authors declare no competing financial interest.

■ ACKNOWLEDGMENTS

This work was funded by Faculty Recruitment Funds (5201030128).

■ REFERENCES

- (1) De Smet, G.; Bai, X.; Maes, B. U. W. Selective C (aryl)–O bond cleavage in biorenewable phenolics. *Chem. Soc. Rev.* **2024**, *53*, 5489–5551.
- (2) Yuan, L.-L.; Wang, H.-M.; Wu, Y.-C.; Hou, Q.-X.; Sun, R.-C. The booming lignin-derived functional composites/nanocomposites. *Composites, Part B* **2024**, *287*, 111869.
- (3) Shen, Y.; Zhou, H.; He, X.; Shen, F.; Xu, Z.; Yang, B.; Kong, L. Z.; Dai, L. Emerging applications of deep eutectic solvents in the preparation and functionalization of biomass-derived carbonaceous materials: challenges and prospects. *Green Chem.* **2024**, *26*, 8123–8144.
- (4) Wang, H.-M.; Yuan, T.-Q.; Song, G.-Y.; Sun, R.-C. Advanced and versatile lignin-derived biodegradable composite film materials toward a sustainable. *Green Chem.* **2021**, *23* (11), 3790–3817.
- (5) Han, Z.-W.; Wang, H.-M.; Chen, X.; Wu, Y.-C.; Hou, Q.-X. Lignin reinforced eco-friendly and functional nanoarchitectonics materials with tailored interfacial barrier performance. *J. Colloid Interface Sci.* **2025**, *684*, 735–757.
- (6) Zhang, Q.; Meng, J.; Tian, Q.; Zhang, L.; Shen, J.; Ni, Y.; Wang, Z. Effect of hemicellulose and its-derived products on the recycling and efficiency of biomass fractionation using lactic acid/choline chloride (DES). *Bioresour. Technol.* **2025**, *430*, 132545.
- (7) Feng, Y.; Eberhardt, T. L.; Meng, F.; Xu, C.; Pan, H. Efficient extraction of lignin from moso bamboo by microwave-assisted ternary deep eutectic solvent pretreatment for enhanced enzymatic hydrolysis. *Bioresour. Technol.* **2024**, *400*, 130666.
- (8) Wang, W.; Xu, Y.; Zhu, B.; Ge, H.; Wang, S.; Li, B.; Xu, H. Exploration of the interaction mechanism of lignocellulosic hybrid systems based on deep eutectic solvents. *Bioresour. Technol.* **2023**, *385*, 129401.
- (9) Wang, L.; Li, X.; Jiang, J.; Zhang, Y.; Bi, S.; Wang, H.-M. Revealing structural and functional specificity of lignin from tobacco stalk during deep eutectic solvents deconstruction aiming to targeted valorization. *Ind. Crops Prod.* **2022**, *180*, 114696.
- (10) Li, P.; Yang, C.; Jiang, Z.; Jin, Y.; Wu, W. Bioproducts, Lignocellulose pretreatment by deep eutectic solvents and related technologies: A review. *J. Bioresour. Bioprod.* **2023**, *8* (1), 33–44.
- (11) Jablonsky, M.; Majova, V.; Ondrigova, K.; Sima, J. Preparation and characterization of physicochemical properties and application of novel ternary deep eutectic solvents. *Cellulose* **2019**, *26*, 3031–3045.

- (12) Wang, N.; Liu, K.; Hou, Z.; Zhao, Z.; Li, H.; Gao, X. The comparative techno-economic and life cycle assessment for multi-product biorefinery based on microwave and conventional hydrothermal biomass pretreatment. *J. Cleaner Prod.* **2024**, *474*, 143562.
- (13) Zhou, C.; Liu, Y.; Ouyang, B.; Lin, S.; Wang, Y. Systematic evaluation of polyol-assisted acidic deep eutectic solvent pretreatment for improving enzymatic hydrolysis of wheat straw. *Ind. Crops Prod.* **2024**, *212*, 118219.
- (14) Zhou, X.; Liu, X.; Zhan, Y.; Bian, H.; Wu, S.; Dai, H.; Liang, F.; Meng, X.; Huang, C.; Fang, G.; et al. A tailored deep eutectic solvent for high-yield conversion of poplar residues to bio-based building blocks at mild conditions. *Chem. Eng. J.* **2024**, *487*, 150407.
- (15) Zhai, Q.; Long, F.; Jiang, X.; Hse, C.-y.; Jiang, J.; Xu, J. Facile and rapid fractionation of bamboo wood with a p-toluenesulfonic acid-based three-constituent deep eutectic solvent. *Ind. Crops Prod.* **2020**, *158*, 113018.
- (16) Zhang, H.; Wu, R.; Chen, X.; Ni, S.; Xu, C.; Fu, Y.; Qin, M.; Zhang, Y. Products, High-efficient fractionation of poplar chips by ternary deep eutectic solvents system for elevating enzymatic hydrolysis. *Ind. Crops Prod.* **2025**, *225*, 120489.
- (17) Zhao, X.; Lyu, G.; Meng, X.; Liu, Y.; Wang, Z.; Yoo, C. G. Novel ternary deep eutectic solvent fractionation for effective utilization of willow. *Bioresour. Technol.* **2024**, *407*, 131148.
- (18) Huang, Y.; Xu, Y.; Zhu, Y.; Huang, R.; Kuang, Y.; Wang, J.; Xiao, W.; Lin, J.; Liu, Z. Improved glucose yield and concentration of sugarcane bagasse by the pretreatment with ternary deep eutectic solvents and recovery of the pretreated liquid. *Bioresour. Technol.* **2022**, *366*, 128186.
- (19) Ding, W.; Huang, L.; Shi, G.; Yan, B.; Zhang, S. Mild one-pot three components fractionation of lignocellulose enhancing by ternary solvents behavior. *Ind. Crops Prod.* **2025**, *226*, 120770.
- (20) Liu, Y.; Deak, N.; Wang, Z.; Yu, H.; Hameleers, L.; Jurak, E.; Deuss, P. J.; Barta, K. Tunable and functional deep eutectic solvents for lignocellulose valorization. *Nat. Commun.* **2021**, *12* (1), 5424.
- (21) Zhang, M.; An, B.; Wu, K.; Zhang, J.; Wang, J.; Liu, Q.; Cui, Y.; Lu, H. Novel ternary deep eutectic solvent for highly efficient dissolution of lignins: Dissolution behavior and mechanism study. *J. Cleaner Prod.* **2024**, *451*, 142116.
- (22) Yao, L.; Cui, P.; Chen, X.; Yoo, C. G.; Liu, Q.; Meng, X.; Xiong, L.; Ragauskas, A. J.; Yang, H. A combination of deep eutectic solvent and ethanol pretreatment for synergistic delignification and enhanced enzymatic hydrolysis for biorefinery process. *Bioresour. Technol.* **2022**, *350*, 126885.
- (23) Ci, Y.-H.; Yu, F.; Zhou, C.-X.; Mo, H.-E.; Li, Z.-Y.; Ma, Y.-Q.; Zang, L.-H. New ternary deep eutectic solvents for effective wheat straw deconstruction into its high-value utilization under near-neutral conditions. *Green Chem.* **2020**, *22* (24), 8713–8720.
- (24) Liu, Z.; Hou, Y.; Hu, S. Rapid microwave-assisted pretreatment using a ternary deep eutectic solvent for lignin fractionation of eucalyptus. *Ind. Crops Prod.* **2024**, *212*, 118297.
- (25) Yu, Y.; Cheng, W.; Li, Y.; Wang, T.; Xia, Q.; Liu, Y.; Yu, H. Tailored one-pot lignocellulose fractionation to maximize biorefinery toward versatile xylochemicals and nanomaterials. *Green Chem.* **2022**, *24* (8), 3257–3268.
- (26) Zhou, C.; Liu, Y.; Ouyang, B.; Lin, S.; Wang, Y. Systematic evaluation of polyol-assisted acidic deep eutectic solvent pretreatment for improving enzymatic hydrolysis of wheat straw. *Ind. Crops Prod.* **2024**, *212*, 118219.
- (27) Zhang, L.; Zhang, C.; Ma, Y.; Zhao, X.; Zhang, X. Lignocellulose pretreatment by Deep eutectic solvent and water binary system for enhancement of lignin extraction and cellulose saccharification. *Ind. Crops Prod.* **2024**, *211*, 118257.
- (28) Kandanelli, R.; Thulluri, C.; Mangala, R.; Rao, P. V.; Gandham, S.; Velankar, H. R. A novel ternary combination of deep eutectic solvent-alcohol (DES-OL) system for synergistic and efficient delignification of biomass. *Bioresour. Technol.* **2018**, *265*, 573–576.
- (29) Wang, J.; Jing, W.; Tian, H.; Liu, M.; Yan, H.; Bi, W.; Chen, D. Y. Investigation of Deep Eutectic Solvent-Based Microwave-Assisted Extraction and Efficient Recovery of Natural Products. *ACS Sustain. Chem. Eng.* **2020**, *8* (32), 12080–12088.
- (30) Poy, H.; Lladosa, E.; Arcis, A.; Gabaldón, C.; Loras, S. Microwave-assisted ternary deep eutectic solvent pretreatment for improved rice straw saccharification under mild pretreatment conditions. *Ind. Crops Prod.* **2023**, *206*, 117639.
- (31) Bessa, W.; Trache, D.; Tarchoun, A. F.; Abdelaziz, A.; Hussin, M. H.; Brosse, N. Unraveling the Effect of kraft and organosolv processes on the physicochemical properties and thermal stability of cellulose and its microcrystals produced from *Eucalyptus globulus*. *Sustainability* **2023**, *15* (4), 3384.
- (32) Xu, H.; Dong, C.; Wang, W.; Liu, Y.; Li, B.; Liu, F. Machine learning prediction of deep eutectic solvents pretreatment of lignocellulosic biomass. *Ind. Crops Prod.* **2023**, *196*, 116431.
- (33) Li, S.; Wang, Y.; Dong, Q.; Yuan, Z.; Mu, T.; Xue, Z.; Cao, L. Polyol-assisted ternary deep eutectic solvent protective lignocellulose pretreatment for high-efficiency xylan utilization and ethanol production. *Carbohydr. Polym.* **2024**, *346*, 122628.
- (34) Gao, Y.; Ozel, M. Z.; Dugmore, T.; Sulaeman, A.; Matharu, A. S. A biorefinery strategy for spent industrial ginger waste. *J. Hazard. Mater.* **2021**, *401*, 123400.
- (35) Lu, H.; Zhang, L.; Yan, M.; Wang, K.; Jiang, J. Screw extrusion pretreatment for high-yield lignocellulose nanofibrils (LCNF) production from wood biomass and non-wood biomass. *Carbohydr. Polym.* **2022**, *277*, 118897.
- (36) Shrestha, B.; Le Brech, Y.; Ghislain, T.; Leclerc, S.; Carré, V.; Aubriet, F.; Hoppe, S.; Marchal, P.; Pontvianne, S.; Brosse, N.; et al. A Multitechnique Characterization of Lignin Softening and Pyrolysis. *ACS Sustain. Chem. Eng.* **2017**, *5* (8), 6940–6949.
- (37) Liu, C.; Li, Z.; Li, M.-C.; Chen, W.; Xu, W.; Hong, S.; Wu, Q.; Mei, C. Lignin-containing cellulose nanofibers made with microwave-aid green solvent treatment for magnetic fluid stabilization. *Carbohydr. Polym.* **2022**, *291*, 119573.
- (38) Lu, Q.-L.; Wu, J.; Li, Y.; Li, L.; Huang, B. One-pot green extraction of high charge density cellulose nanocrystals with high yield for bionanocomposites. *J. Mater. Sci.* **2021**, *56*, 12212–12223.
- (39) Zhang, X.; Zhang, Q.; Cheng, X.; Yu, J.; Zhang, L.; Wang, Z. One-pot strategy to enhance nanofibrillation and esterification of cellulose using ternary deep eutectic solvent. *Ind. Crops Prod.* **2023**, *206*, 117631.
- (40) Yan, M.; Wu, T.; Ma, J.; Lu, H.; Zhou, X. A systematic study of lignocellulose nanofibrils (LCNF) prepared from wheat straw by varied acid pretreatments. *Ind. Crops Prod.* **2022**, *185*, 115126.
- (41) De Melo, E. M.; Clark, J. H.; Matharu, A. S. The Hy-MASS concept: hydrothermal microwave assisted selective scissoring of cellulose for in situ production of (meso) porous nanocellulose fibrils and crystals. *Green Chem.* **2017**, *19* (14), 3408–3417.
- (42) Liu, W.; Jiang, C.; Li, X.; Li, H.; Zhang, Y.; Huang, Y.; Chen, S.; Hou, Q. Microwave-assisted DES fabrication of lignin-containing cellulose nanofibrils and its derived composite conductive hydrogel. *Carbohydr. Polym.* **2024**, *328*, 121741.
- (43) Worku, L. A.; Bachheti, R. K.; Tadesse, M. G. Preparation and characterization of carboxylated cellulose nanocrystals from *Oxytenanthera abyssinica* (Ethiopian lowland bamboo) cellulose via citric acid anhydrous hydrolysis catalyzed by sulfuric acid. *Biomass Convers. Biorefin.* **2024**, *14* (22), 28807–28823.
- (44) Lim, W.-L.; Gunny, A. A. N.; Kasim, F. H.; Gopinath, S. C.; Kamaludin, N. H. I.; Arbain, D. Cellulose nanocrystals from bleached rice straw pulp: acidic deep eutectic solvent versus sulphuric acid hydrolyses. *Cellulose* **2021**, *28* (10), 6183–6199.
- (45) Yang, J.; Zhang, W.; Tang, Y.; Li, M.; Peng, F.; Bian, J. Mild pretreatment with Bronsted acidic deep eutectic solvents for fractionating β -O-4 linkage-rich lignin with high sunscreen performance and evaluation of enzymatic saccharification synergism. *Bioresour. Technol.* **2023**, *368*, 128258.
- (46) Liu, X.; Xie, M.; Hu, Y.; Li, S.; Nie, S.; Zhang, A.; Wu, H.; Li, C.; Xiao, Z.; Hu, C. Facile preparation of lignin nanoparticles from waste *Camellia oleifera* shell: The solvent effect on the structural

characteristic of lignin nanoparticles. *Ind. Crops Prod.* **2022**, *183*, 114943.

(47) Provost, V.; Dumarcay, S.; Ziegler-Devin, I.; Boltoeva, M.; Trébouet, D.; Villain-Gambier, M. Deep eutectic solvent pretreatment of biomass: Influence of hydrogen bond donor and temperature on lignin extraction with high β -O-4 content. *Bioresour. Technol.* **2022**, *349*, 126837.

(48) Shen, X.-J.; Chen, T.; Wang, H.-M.; Mei, Q.; Yue, F.; Sun, S.; Wen, J.-L.; Yuan, T.-Q.; Sun, R.-C. engineering, Structural and morphological transformations of lignin macromolecules during bio-based deep eutectic solvent (DES) pretreatment. *ACS Sustain. Chem. Eng.* **2020**, *8* (5), 2130–2137.

(49) Sun, X.; Zhou, Z.; Tian, D.; Zhao, J.; Zhang, J.; Deng, P.; Zou, H.; Lu, C. Acidic deep eutectic solvent assisted mechanochemical delignification of lignocellulosic biomass at room temperature. *Int. J. Biol. Macromol.* **2023**, *234*, 123593.

(50) Hassanpour, M.; Abbasabadi, M.; Moghaddam, L.; Sun, F. F.; Gebbie, L.; Te'o, V. S. J.; O'Hara, I. M.; Zhang, Z. Mild fractionation of sugarcane bagasse into fermentable sugars and β -O-4 linkage-rich lignin based on acid-catalysed crude glycerol pretreatment. *Bioresour. Technol.* **2020**, *318*, 124059.

(51) Cheng, J.; Huang, C.; Zhan, Y.; Han, S.; Wang, J.; Meng, X.; Yoo, C. G.; Fang, G.; Ragauskas, A. J. Effective biomass fractionation and lignin stabilization using a diol DES system. *Chem. Eng. J.* **2022**, *443*, 136395.

(52) Cheng, J.; Zhan, Y.; Liu, X.; Huang, C.; Zhou, X.; Wang, J.; Meng, X.; Yoo, C. G.; Fang, G.; Ragauskas, A. J. One-pot generation of lignin microspheres and digestible substrate with a polyol-DES pretreatment in high solid loading. *J. Cleaner Prod.* **2023**, *394*, 136322.

(53) Yong, K. J.; Wu, T. Y. Recent advances in the application of alcohols in extracting lignin with preserved β -O-4 content from lignocellulosic biomass. *Bioresour. Technol.* **2023**, *384*, 129238.

(54) Liu, R.; Ding, T.; Deng, P.; Yan, X.; Xiong, F.; Chen, J.; Wu, Z. Biorefinery, Structure and properties of deep eutectic solvent lignin degraded by H_2O_2 . *Biomass Convers. Biorefin.* **2021**, *13*, 12581–12590.

(55) Pang, T.; Wang, G.; Sun, H.; Wang, L.; Liu, Q.; Sui, W.; Parvez, A. M.; Si, C. Lignin fractionation for reduced heterogeneity in self-assembly nanosizing: toward targeted preparation of uniform lignin nanoparticles with small size. *ACS Sustain. Chem. Eng.* **2020**, *8* (24), 9174–9183.

(56) Pylypchuk, I. V.; Karlsson, M.; Lindén, P. A.; Lindström, M. E.; Elder, T.; Sevastyanova, O.; Lawoko, M. Molecular understanding of the morphology and properties of lignin nanoparticles: unravelling the potential for tailored applications. *Green Chem.* **2023**, *25* (11), 4415–4428.

(57) Terzopoulou, Z.; Pappa, C.; Triantafyllidis, K.; Bikiaris, D. N. Unravelling the impact of lignin particle size and content on enhanced value in plastic composites. *Sustain. Chem. Environ.* **2025**, *9*, 100194.



CAS INSIGHTS™

EXPLORE THE INNOVATIONS SHAPING TOMORROW

Discover the latest scientific research and trends with CAS Insights. Subscribe for email updates on new articles, reports, and webinars at the intersection of science and innovation.

Subscribe today

CAS
A Division of the
American Chemical Society